

Wide & Deep neural network model for patch aggregation in CNN-based prostate cancer detection systems

L. Duran-Lopez^{a,b,c,d,*}, Juan P. Dominguez-Morales^{a,b,c,d}, D. Gutierrez-Galan^{a,b,c,d},
A. Rios-Navarro^{a,b,c,d}, A. Jimenez-Fernandez^{a,b,c,d}, S. Vicente-Diaz^{a,b,c,d} and A. Linares-Barranco^{a,b,c,d}

^aRobotics and Tech. of Computers Lab., Universidad de Sevilla, 41012 Seville, Spain

^bEscuela Técnica Superior de Ingeniería Informática (ETSI), Universidad de Sevilla, 41012 Seville, Spain

^cEscuela Politécnica Superior (EPS), Universidad de Sevilla, 41011 Seville, Spain

^dSmart Computer Systems Research and Engineering Lab (SCORE), Research Institute of Computer Engineering (I3US), Universidad de Sevilla, 41012 Seville, Spain

ARTICLE INFO

Keywords:

prostate cancer
deep learning
convolutional neural networks
computer-aided diagnosis
patch aggregation
whole-slide images
medical image analysis

ABSTRACT

Prostate cancer (PCa) is one of the most commonly diagnosed cancer and one of the leading causes of death among men, with almost 1.41 million new cases and around 375,000 deaths in 2020. Artificial Intelligence algorithms have had a huge impact in medical image analysis, including digital histopathology, where Convolutional Neural Networks (CNNs) are used to provide a fast and accurate diagnosis, supporting experts in this task. To perform an automatic diagnosis, prostate tissue samples are first digitized into gigapixel-resolution whole-slide images. Due to the size of these images, neural networks cannot use them as input and, therefore, small subimages called patches are extracted and predicted, obtaining a patch-level classification. In this work, a novel patch aggregation method based on a custom Wide & Deep neural network model is presented, which performs a slide-level classification using the patch-level classes obtained from a CNN. The malignant tissue ratio, a 10-bin malignant probability histogram, the least squares regression line of the histogram, and the number of malignant connected components are used by the proposed model to perform the classification. An accuracy of 94.24% and a sensitivity of 98.87% were achieved, proving that the proposed system could aid pathologists by speeding up the screening process and, thus, contribute to the fight against PCa.

1. Introduction

According to GLOBOCAN, prostate cancer (PCa) is the second most frequently diagnosed cancer and the fifth leading cause of cancer death in men, with more than 1.41 million cases in 2020 and around 375,000 deaths worldwide [1]. It is estimated that PCa cases will increase with around 1,000,000 new cases in 2040, according to the World Health Organization (WHO) [2].

Generally, the first step to diagnose PCa consists in a Digital Rectal Exam (DRE), which is the primary test for the initial clinical assessment of the prostate. If an abnormal result for DRE is found, a Prostate-Specific Antigen (PSA) analysis is performed as a screening method for the investigation of a tumor. Then, in case of a positive PSA, a transrectal ultrasound-guided biopsy is considered, which is the most certainly test to confirm or exclude the presence of cancer [3]. With this technique, prostate samples are obtained, which are processed in a laboratory and scanned, resulting on gigapixel-resolution images called Whole-Slide Images (WSIs). These images are analyzed by pathologists to provide a final diagnosis with the corresponding cancer treatment.

The use of Artificial Intelligence (AI) in image analysis has had a huge impact in recent years [4, 5], mainly due to the computational advances and the accessibility of its algorithms to researchers. Its application in the biomedical field has been expanded considerably, particularly, the use of Deep Learning (DL), which has become one of the most popular AI techniques for image recognition in the last years [6]. These algorithms could play an important role as screening methods in order to report a second opinion and assist doctors in a specific image analysis tasks [7, 8]. Particularly, this approach has recently been widely used in digital histopathology, where Convolutional Neural Networks (CNNs) and other different DL mechanisms are trained to analyze and detect malignant tissue in WSIs. Since CNNs cannot use an entire WSI as input due to their high resolution, which would require a huge memory and processing capacity, a common approach to this problem is to extract smaller subimages from them, called patches. Therefore, the CNN is able to analyze the WSIs at patch level and then report the classification results obtained.

Previous works, such as [9, 10, 11, 12, 13], have followed this patch-level classification strategy in order to develop DL-based Computer-Aided Diagnosis (CAD) systems for PCa detection in digitized histopathological images, reporting accurate results with different metrics and datasets. Among them, to the best of the authors' knowledge, PROM-ETEO [14] achieved the fastest and least complex model [15] while also obtaining state-of-the-art results, leading to the most-plausible edge-computing solution for PCa detec-

*Corresponding author

✉ lduran@atc.us.es (L. Duran-Lopez)

ORCID(s): 0000-0002-5849-8003 (L. Duran-Lopez);

0000-0002-5474-107X (J.P. Dominguez-Morales); 0000-0003-3100-0604 (D.

Gutierrez-Galan); 0000-0003-4163-8484 (A. Rios-Navarro);

0000-0003-3061-5922 (A. Jimenez-Fernandez); 0000-0001-9466-485X (S.

Vicente-Diaz); 0000-0002-6056-740X (A. Linares-Barranco)

tion. This was achieved by means of a 9-layer custom CNN trained and validated with a set of patches after applying different processing steps, including patch filtering, stain normalization and data augmentation. This allowed achieving 99.98% accuracy, 99.98% F1 score and 0.999 Area Under Curve (AUC) on a separate test set.

Since the results obtained when using CNNs are reported at patch level, different techniques have been proposed in the literature in order to combine them and generate a slide-level classification result, which could be of great importance for developing a fast PCa screening system. This technique is known as patch aggregation. Among the different studies that can be found in the literature, some performed different patch aggregation techniques based on Recurrent Neural Networks (RNNs) [10], Random Forests (RFs) [10] an other Machine Learning (ML) or statistical alternatives [9, 13], achieving accurate solutions and leading to precise screening methods that could help pathologists in their task.

In this work, a custom novel Wide & Deep (W&D) model for aggregating the patch-level classification results obtained from the PROMETEO CAD system into a global slide-level class is presented. This approach allows providing a fast screening method for PCa detection at WSI level, while also benefiting from the spatial resolution obtained at patch level. The promising results obtained, which have also been compared to other state-of-the-art ML-based approaches, show that the proposed solution could aid pathologists when analyzing histopathological images, discriminating between positive and negative PCa samples while fastening up the whole process.

The main contributions of this work include the following:

- A set of algorithms to automatically extract relevant features from the output of a patch-level DL-based PCa detection system.
- A 5-layer custom W&D model, trained and validated from scratch, which extracts independent features from the inputs and combine them to achieve a slide-level PCa screening method with high sensitivity.
- A comparative study between different widely-known ML algorithms for the patch-aggregation task on the same dataset, which shows that the proposed method achieves the highest sensitivity.

The rest of the paper is structured as follows: in section 2, the materials and methods are presented, focusing on the dataset that was used for this work (2.1), along with the neural network model (2.2), and the details on the training and validation steps of the model with the aforementioned dataset (2.3). Then, section 3 presents the results obtained with the proposed model using different evaluation metrics. A comparison with other state-of-the-art ML techniques is also performed in the same section. Finally, the conclusions of this work are presented in section 4.

2. Materials and Methods

2.1. Dataset

A set of Hematoxylin and Eosin (H&E)-stained slides were used (158 normal WSIs and 174 malignant WSIs) provided by the Pathological Anatomy Unit of Virgen de Valme Hospital (Sevilla, Spain). These images were preprocessed using different steps. First, small subimages, called patches (100×100 pixels at 10× magnification), were extracted from them. Next, background patches and patches corresponding to unwanted areas were discarded with a filter that discriminates them based on the amount of tissue that they contain, the percentage of pixels that are within H&E's hue range, and the dispersion of the saturation and brightness channels. Then, a color normalization process called Reinhard stain-normalization [16, 17] was applied to patches in order to reduce stain variability between samples. Finally, color-normalized patches were used as input to a CNN, called PROMETEO, which classifies them as either malignant or normal tissue with a certain probability. A deeper insight on these steps is given in [14] and can be seen in Fig. 1.

Different features were obtained from PROMETEO's output in order to create the dataset. The first feature considered to discriminate between malignant or normal WSI was the percentage of malignant tissue area, also called malignant tissue ratio (MTR), expressed between 0 and 1. This was calculated by dividing the number of patches classified as malignant by the total amount of tissue patches extracted from the WSI. This is the most representative data to perform a slide-level classification, since the more malignant patches the network detects on the WSI, the more likely it is of being malignant. However, based on the error of the CNN when performing the patch classification, the percentage of malignant tissue of the WSI should not be the only input to be considered for the patch aggregation task, since there are some exceptions that do not meet the aforementioned rule (e.g. a malignant WSI with a small tumor in a specific region or a normal WSI with a relatively high percentage of incorrectly-classified malignant tissue area).

Therefore, another feature taken into account to distinguish between malignant and normal WSIs was the distribution of the prediction probability for malignant patches. When the CNN predicts a patch, it reports the probability of the patch for being either malignant or normal. If we only focus on the malignant probability, the network should have a higher confidence for patches corresponding to malignant tissue than for those corresponding to normal tissue that have been incorrectly predicted as malignant. Thus, a 10-bin histogram with the prediction probabilities of the patches classified as malignant for each WSI was calculated. These probabilities were distributed from 50% to 100%, with 5% range for each bin. The histogram was normalized with respect to the total number of tissue patches. Along with the malignant probability histogram (MPH), the least squares regression line (LSRL) of the histogram, defined as $y = mx + b$, was also calculated, where m and b , which refer to the slope and the Y-intercept, are described in equations 1 and 2, re-

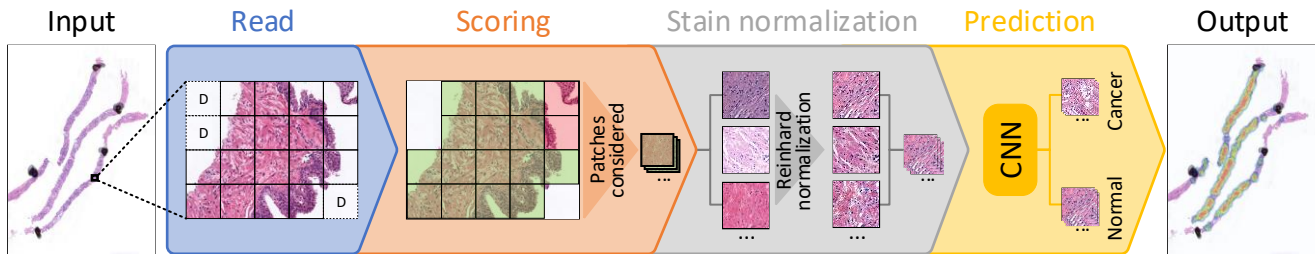


Figure 1: Block diagram detailing each of the steps considered for processing a whole-slide image (WSI) in PROMETEO. First, in the step called *Read*, patches are extracted from the input WSI, and those corresponding to background are discarded (those identified as D). Then, in the next step, a score is given to each patch in order to discard patches corresponding to unwanted areas, such as pen marks and external agents. This score discriminates considering three factors: the amount of tissue that the patch contains, the percentage of pixels that are within H&E's hue range, and the dispersion of the saturation and brightness channels. Discarded patches in this step are shown in red, while those that pass the scoring filter are highlighted in green. The third step, called *Stain normalization*, applies a color normalization to the patches based on Reinhard's stain-normalization method in order to reduce color variability between samples. Finally, in the *Prediction* step, each of the patches are used as input to the CNN, which classifies them as either malignant or normal tissue. A deeper insight on these steps is given in [14].

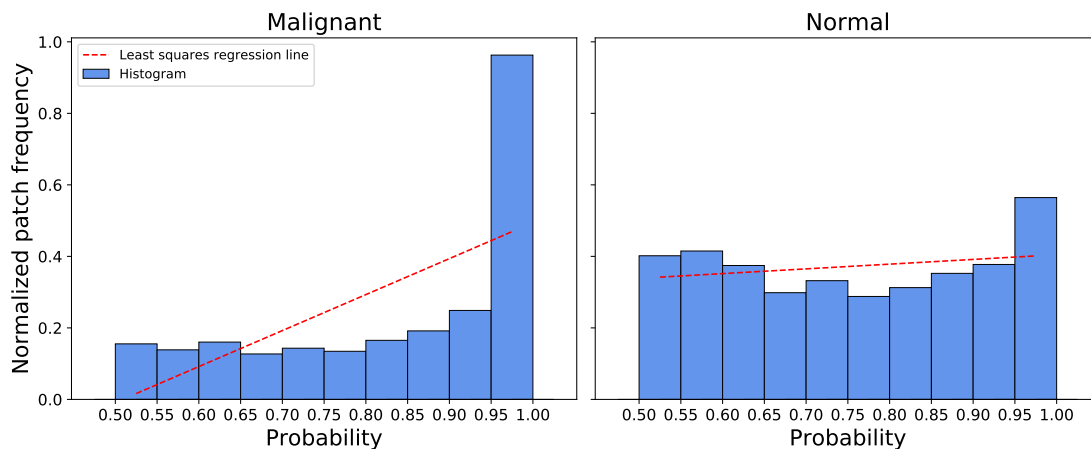


Figure 2: Mean probability histogram of the normalized patch frequency across all the WSIs, distinguishing between malignant (left) and normal (right) samples. The least squares regression line is shown with a red dashed line. As can be seen, for malignant WSIs, the system tends to classify patches as malignant with a higher confidence. This produces a least squares regression line with a steeper slope. On the other hand, for the normal WSIs, the classification for malignant patches is not that accurate, which leads to a less steep regression line.

spectively. This line represents the best approximation of the set of probabilities for all malignant patches of the corresponding WSI. The mean histogram for both malignant and normal WSIs are shown in Fig. 2 together with their corresponding LSRLs, which are highlighted in red.

$$m = \frac{N \sum x_i y_i - \sum x_i \sum y_i}{N \sum x_i^2 - (\sum x_i)^2} \quad (1)$$

$$b = \frac{N \sum x_i^2 \sum y_i - \sum x_i \sum x_i y_i}{N \sum x_i^2 - (\sum x_i)^2} \quad (2)$$

Where x and y represent the coordinates of the different values of the histogram.

As it was previously mentioned, the error of the ML algorithm (a CNN in this case) leads to errors in the classi-

fication, which in a WSI is presented as sparse normal tissue patches being classified as malignant. Therefore, in a WSI diagnosed as normal, patches classified as malignant by the CNN are sparsely distributed through the tissue. On the other hand, in a cancerous WSI, malignant-classified patches tend to be focused around the tumor areas. Due to this reason, the dispersion factor of malignant-classified patches was also considered as another relevant input for the slide-level classification between normal and malignant WSIs. This factor was obtained by calculating the number of malignant connected components (MCC), which counts the isolated components (sets of malignant patches) in the classification result according to a specific distance D . Algorithm 1 details the method used to calculate the number of connected components based on the center coordinates of malignant patches and D . In this work, five different values were con-

Algorithm 1: Connected components algorithm**ConnectedPatches** (*centers*, *D*)**inputs :** A list of center points from malignant patches (*centers*); a distance (*D*).**output:** A set of lists of connected patch centers with relative distance *D*.

```

connected_components = [];
current_component = [];
while count(centers) > 0 do
  current_component = [];
  current_component.append(centers[0]);
  centers.remove(centers[0]);
  foreach center in current_component do
    foreach point in centers do
      if distance from center to point <= D then
        current_component.append(point);
        centers.remove(point);
    end
  end
  connected_components.append(current_component);

```

sidered for D (142, 283, 425, 566 and 708 pixels), which correspond to the Euclidean distances (i.e., radii) from a patch to a range of 1 up to 5 patches-distance, taking into account that the distance between two patches is 100 pixels (patches are 100×100 pixels size). The number of connected components was normalized with respect to the total number of malignant patches for each WSI. This way, normal samples with a low quantity of sparse misclassifications are penalized when compared to malignant samples with sparse tumoral tissue regions.

2.2. Wide & Deep network model

The dataset described in section 2.1 was used as input to a Neural Network (NN) model called W&D [18] to provide a slide-level classification between normal and malignant WSIs. The W&D model combines both wide and deep components. The wide component memorizes sparse interactions between features effectively, which can be defined as learning how the output responds to combinations of sparse input values. On the other hand, the deep component corresponds to the feed-forward neural network which represents the generalization, this is, the ability to handle unseen data. Therefore, the benefits from both memorization (wide) and generalization (deep) are combined and achieved in a single model [18].

In this work, the malignant tissue ratio was used as the wide element while the malignant probability histogram, the slope and Y-intercept of the LSRL and the number of malignant connected components were used as the deep elements. Each of the deep data were separately connected to two hidden layers of 300 neurons. Then, these layers were concatenated together with the wide element to a hidden block of two hidden layers with 300 neurons each. Finally, this hidden block was connected to the output layer, a SoftMax function which performs the classification of the WSI as either malignant or normal. This way, complex features are extracted from combinations of sparse inputs and then con-

catenated together in order to perform the final decision.

Figure 3 depicts the custom W&D model used in this work, where the different inputs and layers can be seen. Figure 4 represents the whole processing step for the prostate screening task, highlighting both the patch-level and the slide-level components.

2.3. Training and validation

K-fold stratified cross-validation was performed to measure the generalization ability of the model. This technique consisted in dividing the dataset in 5 sets ($K = 5$). For each fold, the network was trained using four of the five sets (80% of the dataset) for 10000 epochs and validated using the remaining one (20% of the dataset). This way, for each experiment, the network was trained and validated a total of five times with different data. The final results are presented as the mean accuracy calculated over the five cross-validation folds.

To validate the network, different evaluation metrics were used. These were the accuracy (eq. 3), sensitivity (eq. 4), precision (eq. 5), F1 score (eq. 6) and AUC of the Receiver Operating Characteristic (ROC) curve.

$$\text{Accuracy} = 100 \times \frac{\text{TP} + \text{TN}}{\text{TP} + \text{TN} + \text{FP} + \text{FN}} \quad (3)$$

$$\text{Sensitivity} = 100 \times \frac{\text{TP}}{\text{TP} + \text{FN}} \quad (4)$$

$$\text{Precision} = 100 \times \frac{\text{TP}}{\text{TP} + \text{FP}} \quad (5)$$

$$\text{F1 score} = 2 \times \frac{\text{Precision} \times \text{Sensitivity}}{\text{Precision} + \text{Sensitivity}} \quad (6)$$

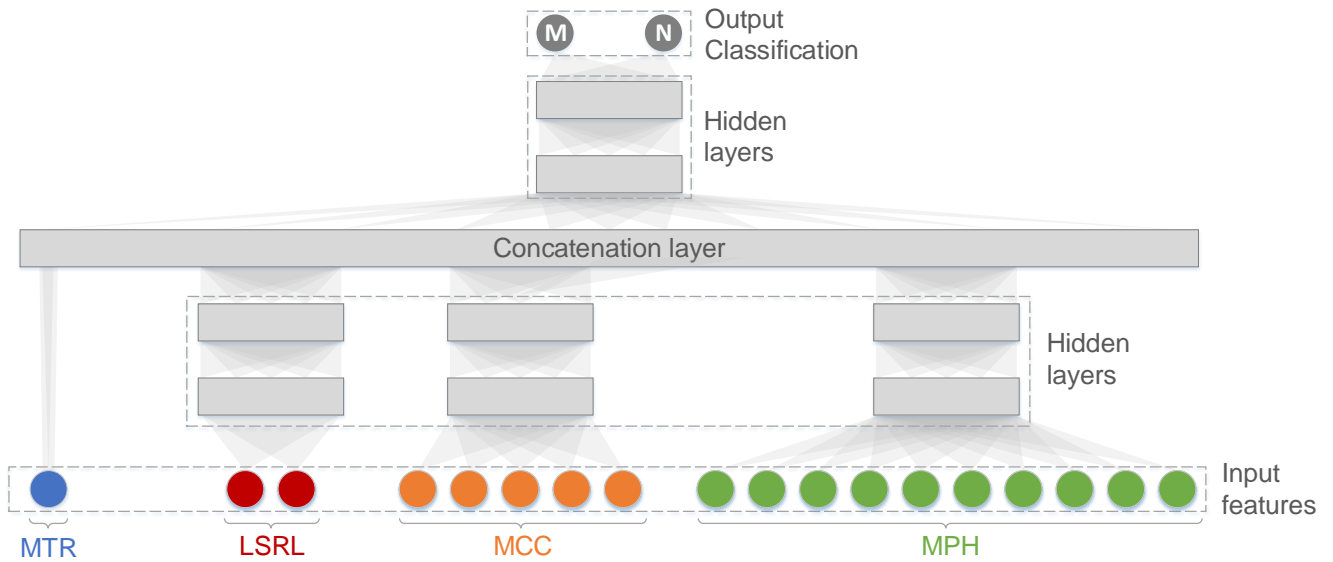


Figure 3: Diagram of the W&D network model proposed in this work. Each hidden layer consists of 300 neurons. The input features, which are detailed in section 2.1, are: the malignant tissue ratio (MTR) of the WSI, the slope and Y-intercept of the least squares regression line (LSRL) of the histogram, the number of malignant connected components (MCC) with 5 different radii (from 1 to 5 malignant patch distance), and the 10-bin malignant probability histogram (MPH) between 50% and 100% with 5% ticks. These input features are used to classify the WSI as either malignant (M) or normal (N).

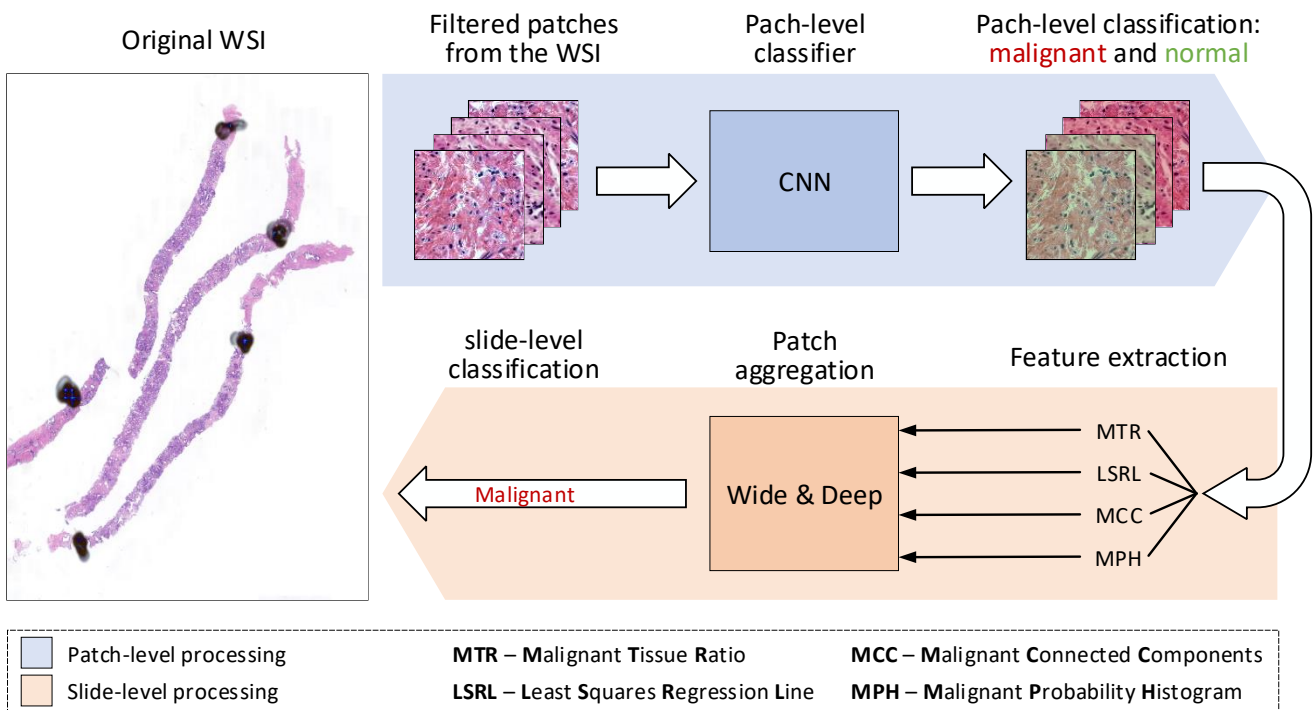


Figure 4: Diagram of the whole processing step for the PCa screening task. First, the WSI is processed at patch level, following the same procedure presented in Figure 1. Then, the output classification for each of the filtered patches from the original WSI is used to perform a slide-level prediction using the W&D model presented in Figure 3, where the extracted features are used to classify the WSI as either malignant or normal.

Where TP and FP denote true positive cases (when the model diagnoses a malignant WSI correctly) and false positive cases (the network diagnoses a normal WSI as malignant), respectively. TN and FN denote true negative cases (the system classifies a normal WSI as normal) and false negative cases (the network classifies a malignant WSI as normal), respectively.

For designing, training and validating the model, both TensorFlow¹ and Keras² were used.

3. Results and Discussion

After training the custom W&D model (section 2.2) with the dataset presented in section 2.1, all the different metrics described in section 2.3 were calculated and obtained in order to evaluate the proposed system. Table 1 summarizes the results for each cross-validation fold together with the average for all the evaluation metrics. With these, the average results were calculated, achieving an accuracy of 94.24%, a sensitivity of 98.87%, a precision of 90.23%, a F1 score of 94.33% and an AUC of 0.94.

Table 1
Validation results obtained with the proposed W&D model. The accuracy, sensitivity, precision, F1 score and AUC are shown for each of the different cross-validation folds. The average of the obtained metrics across the five folds is also presented.

Fold	Accuracy (%)	Sensitivity (%)	Precision (%)	F1 score (%)	AUC
1	93.93	100	89.74	94.59	0.93
2	93.93	97.29	92.30	94.73	0.93
3	95.45	100	90.32	94.91	0.96
4	93.93	100	87.09	93.10	0.94
5	93.93	97.05	91.66	94.28	0.93
Average	94.24	98.87	90.23	94.33	0.94

As can be seen, the results obtained across the different folds are consistent and the proposed model achieves very high scores in all the different metrics studied for this classification task, particularly in terms of sensitivity. The sensitivity, which in this field is defined as the ability of the system to identify PCa, is of utmost importance for reporting and assessing the performance of the screening test [19]. The proposed system is able to achieve an average sensitivity of around 99%, where three of the folds achieved perfect sensitivity (100%). This means that our custom model makes almost no mistakes when predicting a malignant sample as such, making it a reliable patch aggregation method, together with PROMETEO, for PCa detection in WSIs. Figure 5 shows some examples of correctly classified WSIs.

The results obtained in this study were compared with different ML-based methods and classifiers using the same dataset. The following well-known machine learning algorithms were used to classify the WSIs: an Artificial Neural Network (ANN) [20], a Support Vector Machine (SVM)

[21], a RF [22] and a k-Nearest Neighbors (KNN) [23]. Table 2 summarizes the results obtained for each method, which are represented as the average of the evaluation metrics (see section 2.3) obtained for each cross-validation fold.

As it can be seen, the best results for accuracy, sensitivity, F1 score and AUC are obtained with the proposed W&D model, with the exception of precision, for which SVM achieves the highest value. As it was previously mentioned, sensitivity is the most relevant metric for measuring the performance of a classifier when performing a screening test. In this case, the proposed architecture is the one achieving the highest sensitivity score among the different algorithms evaluated, with a difference of more than 6% with the second highest, which is the ANN. On the other hand, SVM achieves around 99% precision, which could be very relevant for other binary or multi-class classification tasks, but not as much as the sensitivity when developing a ML-based PCa screening method that could help experts in order to accelerate the whole process.

4. Conclusions

In this work, the authors present a novel ML-based method to classify WSIs of prostate tissue as normal or malignant at global slide level based on a previous patch-level classification. This classification is based on a novel NN model called W&D, which combines both linear model components (wide) and neural network components (deep) in order to achieve both memorization and generalization in a single model. The custom W&D proposed model classifies each WSI as normal or malignant considering different processed inputs. This information was obtained using PROMETEO, a CAD system which extracts small patches from WSIs which are first preprocessed and then classified, reporting a heatmap that shows where malignant areas are located inside the corresponding WSI. From the information obtained from malignant patches, different processed features are calculated, which are then used as input to the proposed W&D model. These are the malignant tissue ratio, the 10-bin malignant probability histogram between 50% and 100% with 5% ticks, the slope and Y-intercept of the least squares regression line of the histogram and the number of malignant connected components with 5 different radii. The network was trained and validated using 5-fold cross-validation. The average results obtained for the cross-validation sets with the W&D model achieved an accuracy of 94.24%, a sensitivity of 98.87%, a precision of 90.23%, a F1 score of 94.33% and an AUC of 0.94. The proposed model was compared with other state-of-the-art methods (ANN, SVM, RF and KNN) using the same dataset. The results show that the W&D model performs better in terms of accuracy, sensitivity, F1 score and AUC. The promising results obtained with this novel model show that the proposed system could aid pathologists when analyzing histopathological images as a screening method, discriminating between normal and malignant PCa slides.

¹<https://www.tensorflow.org> (accessed May 24, 2021)

²<https://keras.io> (accessed May 24, 2021)

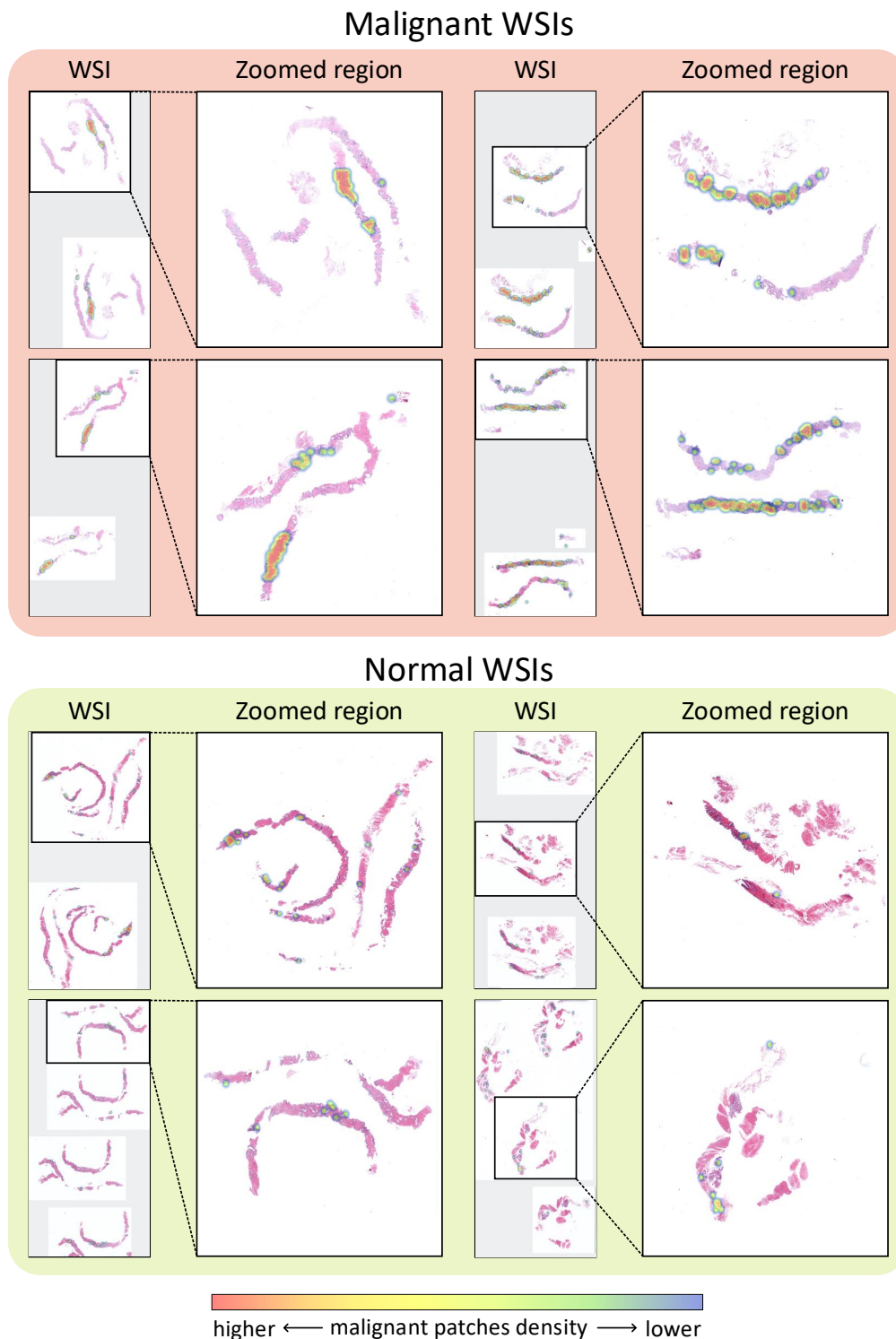


Figure 5: Eight different WSI samples extracted from the dataset presented in section 2.1. A heatmap of the malignant patches predicted by PROMETEO is drawn on top of the WSI, and zoomed regions are presented for better visualization. Red regions represent higher concentrations of malignant patches, while blue represent the opposite. The examples presented were correctly classified by the proposed W&D model.

Acknowledgments

We would like to thank Antonio Felix Conde-Martin and the Pathological Anatomy Unit of Virgen de Valme Hospi-

tal in Seville (Spain) for their support in the PROMETEO project, together with VITRO S.A., along with providing us with annotated WSIs from the same hospital. The authors would like to thank the Spanish Agencia Estatal de

Table 2

Validation results calculated from the average of the evaluation metrics (accuracy, sensitivity, precision, F1 score and AUC) for the 5 different cross-validation sets. The results obtained with the proposed W&D model are compared to other state-of-the-art ML-based algorithms, namely, ANN, SVM, RF and KNN. The best result for each specific evaluation metric is highlighted in bold.

Model	Accuracy (%)	Sensitivity (%)	Precision (%)	F1 score (%)	AUC
W&D (proposed)	94.24	98.87	90.23	94.33	0.94
ANN	89.69	92.47	87.29	89.54	0.89
SVM	88.18	80.78	98.76	88.79	0.89
RF	88.84	84.89	92.23	88.22	0.88
KNN	88.48	83.29	94.31	88.31	0.88

Investigación (AEI) for supporting this work. This work was partially funded by Spanish Agencia Estatal de Investigación (AEI) project MINDROB (PID2019-105556GB-C33/AEI/10.13039/501100011033), with support from the European Regional Development Fund, by the EU H2020 project CHIST-ERA SMALL (PCI2019-111841-2) and by the Andalusian Regional Project PAIDI2020 (with FEDER support) PROMETEO (AT17_5410_USE).

References

- [1] Hyuna Sung, Jacques Ferlay, Rebecca L Siegel, Mathieu Laversanne, Isabelle Soerjomataram, Ahmedin Jemal, and Freddie Bray. Global cancer statistics 2020: Globocan estimates of incidence and mortality worldwide for 36 cancers in 185 countries. *CA: A Cancer Journal for Clinicians*, 2021.
- [2] Prashanth Rawla. Epidemiology of prostate cancer. *World journal of oncology*, 10(2):63, 2019.
- [3] Nigel Borley and Mark R Feneley. Prostate cancer: diagnosis and staging. *Asian journal of andrology*, 11(1):74, 2009.
- [4] Pavel Hamet and Johanne Tremblay. Artificial intelligence in medicine. *Metabolism*, 69:S36–S40, 2017.
- [5] Abhimanyu S Ahuja. The impact of artificial intelligence in medicine on the future role of the physician. *PeerJ*, 7:e7702, 2019.
- [6] Dinggang Shen, Guorong Wu, and Heung-Il Suk. Deep learning in medical image analysis. *Annual review of biomedical engineering*, 19:221–248, 2017.
- [7] Geert Litjens, Thijs Kooi, Babak Ehteshami Bejnordi, Arnaud Arindra Adiyoso Setio, Francesco Ciompi, Mohsen Ghafoorian, Jeroen Awm Van Der Laak, Bram Van Ginneken, and Clara I Sánchez. A survey on deep learning in medical image analysis. *Medical image analysis*, 42:60–88, 2017.
- [8] A Fourcade and RH Khonsari. Deep learning in medical image analysis: A third eye for doctors. *Journal of stomatology, oral and maxillofacial surgery*, 120(4):279–288, 2019.
- [9] Peter Ström, Kimmo Kartasalo, Henrik Olsson, Leslie Solorzano, Brett Delahunt, Daniel M Berney, David G Bostwick, Andrew J Evans, David J Grignon, Peter A Humphrey, et al. Artificial intelligence for diagnosis and grading of prostate cancer in biopsies: a population-based, diagnostic study. *The Lancet Oncology*, 21(2):222–232, 2020.
- [10] Gabriele Campanella, Matthew G Hanna, Luke Geneslaw, Allen Miralflor, Vitor Werneck Krauss Silva, Klaus J Busam, Edi Brogi, Victor E Reuter, David S Klimstra, and Thomas J Fuchs. Clinical-grade computational pathology using weakly supervised deep learning on whole slide images. *Nature medicine*, 25(8):1301–1309, 2019.
- [11] Geert Litjens, Clara I Sánchez, Nadya Timofeeva, Meyke Hermsen, Iris Nagtegaal, Iring Kovacs, Christina Hulsbergen-Van De Kaa, Peter Bult, Bram Van Ginneken, and Jeroen Van Der Laak. Deep learning as a tool for increased accuracy and efficiency of histopathological diagnosis. *Scientific reports*, 6(1):1–11, 2016.
- [12] Wenyuan Li, Jiayun Li, Karthik V Sarma, King Chung Ho, Shiwen Shen, Beatrice S Knudsen, Arkadiusz Gertych, and Corey W Arnold. Path r-cnn for prostate cancer diagnosis and gleason grading of histological images. *IEEE transactions on medical imaging*, 38(4):945–954, 2018.
- [13] Wouter Bulten, Hans Pinckaers, Hester van Boven, Robert Vink, Thomas de Bel, Bram van Ginneken, Jeroen van der Laak, Christina Hulsbergen-van de Kaa, and Geert Litjens. Automated deep-learning system for gleason grading of prostate cancer using biopsies: a diagnostic study. *The Lancet Oncology*, 21(2):233–241, 2020.
- [14] Lourdes Duran-Lopez, Juan P Dominguez-Morales, Antonio Felix Conde-Martin, Saturnino Vicente-Diaz, and Alejandro Linares-Barranco. Prometeo: A cnn-based computer-aided diagnosis system for wsi prostate cancer detection. *IEEE Access*, 8:128613–128628, 2020.
- [15] Lourdes Duran-Lopez, Juan P. Dominguez-Morales, Antonio Rios-Navarro, Daniel Gutierrez-Galan, Angel Jimenez-Fernandez, Saturnino Vicente-Diaz, and Alejandro Linares-Barranco. Performance evaluation of deep learning-based prostate cancer screening methods in histopathological images: Measuring the impact of the model’s complexity on its processing speed. *Sensors*, 21(4), 2021.
- [16] Erik Reinhard, Michael Adhikhmin, Bruce Gooch, and Peter Shirley. Color transfer between images. *IEEE Computer Graphics and Applications*, 21(5):34–41, 2001.
- [17] Derek Magee, Darren Treanor, Doreen Crellin, Mike Shires, Katherine Smith, Kevin Mohee, and Philip Quirke. Colour normalisation in digital histopathology images. In *Proc. Optical Tissue Image analysis in Microscopy, Histopathology and Endoscopy (MICCAI Workshop)*, volume 100, pages 100–111. Citeseer, 2009.
- [18] Heng-Tze Cheng, Levent Koc, Jeremiah Harmsen, Tal Shaked, Tushar Chandra, Hrishi Aradhya, Glen Anderson, Greg Corrado, Wei Chai, Mustafa Ispir, et al. Wide & deep learning for recommender systems. In *Proceedings of the 1st workshop on deep learning for recommender systems*, pages 7–10, 2016.
- [19] Matti Hakama, Anssi Auvinen, Nicholas E Day, and Anthony B Miller. Sensitivity in cancer screening. *Journal of Medical Screening*, 14(4):174–177, 2007.
- [20] Bayya Yegnanarayana. *Artificial neural networks*. PHI Learning Pvt. Ltd., 2009.
- [21] Lipo Wang. *Support vector machines: theory and applications*, volume 177. Springer Science & Business Media, 2005.
- [22] Leo Breiman. Random forests. *Machine learning*, 45(1):5–32, 2001.
- [23] Liangxiao Jiang, Zhihua Cai, Dianhong Wang, and Siwei Jiang. Survey of improving k-nearest-neighbor for classification. In *Fourth international conference on fuzzy systems and knowledge discovery (FSKD 2007)*, volume 1, pages 679–683. IEEE, 2007.